Engineering Structures 160 (2018) 243–256

Contents lists available at ScienceDirect

Engineering Structures

journal homepage: www.elsevier.com/locate/engstruct

Seismic behavior of shear walls with boundary CFST columns and embedded multiple steel plates: Experimental investigation

Qi-Yun Qiao, Wan-Lin Cao*, Xiang-Yu Li, Hong-Ying Dong, Wen-Wen Zhang, Fei Yin

College of Architecture and Civil Engineering, Beijing University of Technology, Beijing 100124, PR China

ARTICLE INFO

Keywords:
Shear wall
Multiple steel plates
Boundary CFST columns
Seismic behavior
Retrofitting

ABSTRACT

In this study, an innovative composite shear wall, comprised of boundary Concrete Filled Steel Tubular (CFST) columns, and Reinforced Concrete (RC) walls embedded with multiple steel plates has been developed. Seven specimens were investigated by cyclic loading tests. The parameters were the type of the boundary CFST columns, the number of multiple steel plates and the axial force ratio. There were two loading stages for the tests. During stage 1, the specimens were tested until a 2.0% drift ratio was attained. After stage 1, damaged specimens were retrofitted and tested in stage 2. The failure characteristics, hysteretic behavior, strength and deformation, strains, energy dissipation capacity and stiffness were studied. The results show that the hysteresis curves of the innovative shear walls were stable. The embedded multiple steel plates had a considerable effect on the seismic behavior of the innovative shear walls, and the strength increased with increasing number of steel plates. There was no considerable difference in the effect on seismic behavior for the different types of the boundary CFST columns. The developed shear walls, after retrofitting, were shown to satisfy seismic requirements. Finally, an evaluation method for the ultimate strength of the shear walls was developed with adequate accuracy.

1. Introduction

Reinforced concrete (RC) shear walls are commonly used in high-rise buildings as they are important components for resisting earthquakes [1,2]. However, in most cases, the axial force ratio of the shear walls is limited according to the seismic design codes of different countries [3–5]. In high-rise buildings, the axial force in the low stories is usually very large. As a result, the wall needs to be designed with dense reinforcing bars and thick sections. The consequences are that it will be more difficult to layout the reinforcing bars, and it also amplifies the earthquake action due to the increase in weight of the structure. Furthermore, increasing the wall thickness reduces the available area. Hence, in high-rise buildings, the design and construction of RC shear walls is very difficult. Sometimes, it is even impossible.

To overcome the RC shear walls' problems mentioned above, Steel Plates Embedded Reinforced Concrete (SPE-RC) shear walls have been developed in recent years [6], and the design provisions are specified in the Chinese code [7]. Fig. 1(a) shows the schematic view of a traditional SPE-RC shear wall. Usually, for an SPE-RC shear wall, the main components are the embedded single full-size steel plate, RC wall and boundary CFST columns [8–11]. However, traditional SPE-RC shear walls have the following disadvantages: (1) The embedded single steel plate is continuous and the size of the entire wall, as such, it is difficult to hoist, to place into its desired location, and to weld. (2) As the embedded single steel plate separates the concrete into two parts, when the shear wall is under a large axial force, the concrete wall may be split into two. In order to prevent the wall from splitting and to improve integration, shear studs or bolts are welded on both sides of the steel plate. However, the cost of welding the shear studs is high and the construction is difficult.

In this study, an innovative shear wall with boundary CFST columns and embedded multiple steel plates has been developed based on the traditional SPE-RC shear wall. Fig. 1(b) shows the schematic view of the innovative composite shear wall. As shown, instead of the single full-size steel plate in the traditional SPE-RC shear wall, multiple steel plates are embedded inside the walls. As compared to a single steel plate, the merits of the multiple steel plates are as follows: (1) Less steel required. (2) As the multiple steel plates are smaller and lighter than the single full-size steel plate, they are easier to hoist, to place into the desired locations and to weld, leading to an easier construction. (3) The integrity of the concrete wall is improved because concrete on the two sides is connected through the gaps between the multiple steel plates. (4) The construction work is simplified because there is no need for welding shear studs or bolts to the steel plate.

In the middle of the innovative shear wall, as shown in Fig. 1(b), an additional boundary CFST column is used to enhance ductility and to

* Corresponding author.
E-mail address: wlcao@bjut.edu.cn (W.-L. Cao).

https://doi.org/10.1016/j.engstruct.2018.01.040
Received 18 May 2017; Received in revised form 11 January 2018; Accepted 12 January 2018

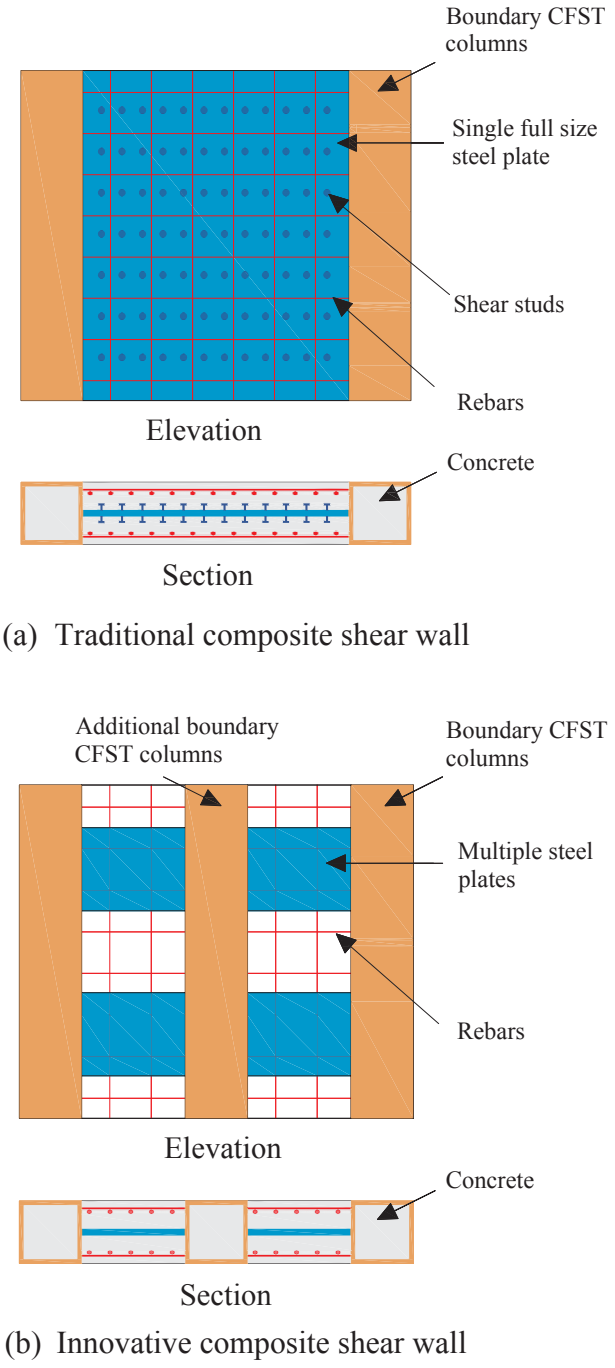

Fig. 1. Schematic view of the traditional and innovative SPE-RC shear wall.

carry part of the axial load. Since the RC wall was divided into two slender walls by the additional boundary CFST column, the displacement capacity of the shear wall can be increased. In Ref. [12], the I-shaped steel was used in the middle of the shear wall to form the Steel Reinforced Concrete (SRC) column. The test results showed that the middle SRC column experienced severe damages. Furthermore, the construction of the SRC column is difficult in engineering practice. In order to overcome these problems, this study used the CFST column rather than the SRC column, as shown in Fig. 1(b).

The present paper reports the cyclic tests of seven innovative shear walls. There were two loading stages for the tests. During stage 1, the specimens were tested until a 2.0% drift ratio was attained. After stage 1, damaged specimens were retrofitted and tested in stage 2. The failure characteristics, hysteretic behavior, strength and deformation, strains, energy dissipation capacity and stiffness were studied. An evaluation method for ultimate strength was developed.

2. Experimental program

2.1. Design of test specimens

A total of seven specimens were designed at approximately 1:5 scale. Table 1 and Fig. 2 show the details of the specimens. The parameters varied for the test were: (1) Number of embedded multiple steel plates m, where m = 0, 2, 3, 4; while specimen S5N1 had a single full-size steel plate to compare the traditional approach to the innovative shear walls with multiple steel plates proposed; (2) The boundary CFST columns type, i.e. square or circular CFST columns; (3) Whether retrofitting work was performed; (4) Axial force ratio n = 0.15 or 0.25. In accordance with the JGJ 3-2011 provisions [13], the axial force ratio n was calculated as follows:

$$n = N/(f_c' A_c + f_y A_s) \quad (1)$$

where N is the axial force, A_c is the concrete area; f_c' is the concrete cylinder compressive strength; f_y is the yield strength of steel; A_s is the total steel area.

Specimen S0N2R is used as an example to explain the specimens' ID in Table 1. (1) S refers to square CFST column, while C refers to circular CFST column; (2) 0 refers to the absence of steel plates, while 2 refers to two steel plates, 3 refers to three steel plates, 4 refers to four steel plates and 5 refers to a single full-size steel plate; (3) N refers to a normal axial force ratio = 0.15, while H refers to a higher axial force ratio = 0.25; (4) 2 refers to stage 2, while 1 refers to stage 1; (5) R refers to a retrofitted specimen.

The overall dimensions of the wall were 960 mm in height and 740 mm in width. The aspect ratio (i.e., height-to-width ratio) was approximately 1.5. The thickness of the RC wall was 140 mm. The loading beams and foundations consisted of rectangular steel boxes filled with concrete. The sizes of the square and circular steel tubes were 140 mm × 140 mm × 4 mm and 160 mm × 5 mm, respectively. The embedded multiple steel plates and CFST columns were connected by full penetration welding. Each steel plate was 160 mm × 160 mm × 4 mm. Fig. 2(c) shows the core steel structure of the specimens.

Reinforcing bars D4 (4 mm diameter) were used for horizontal and vertical reinforcement in the RC wall. The horizontally-distributed bars were welded to the steel tubes. To improve the integrity between the multiple steel plates and the concrete, D4 (4 mm diameter) tie bars were installed through the gaps between the steel plates.

In order to ensure proper anchorage, the vertically distributed reinforcing bars and boundary steel tubes were extended to the bottom of the foundation and the top of the loading beam. Furthermore, three D25 (25 mm diameter) reinforcing bars were inserted through the steel tubes inside the foundation and two inside the loading beam to enhance the anchoring of the walls. Bolts (6 mm in diameter, spaced 60 mm on center) were welded to the steel tubes along the interface between the steel tubes and the RC walls, to enhance the bonding and friction, as shown in Fig. 2(d).

2.2. Material properties

2.2.1. Concrete

The CFST columns, shear walls, foundation and loading beam were cast with the same concrete. The strength grade of the concrete used was C45 according to the Chinese code [14] (i.e. the nominal cubic compressive strength f_{cu}^{150} = 45.3 N/mm^2). In the Chinese codes, cubic tests are performed on 150 mm × 150 mm × 150 mm cylinders. The concrete cylinder compressive strength f_c' can be calculated based on Eq. (2)[14]. According to this equation, the concrete cylinder

Table 1
Specimen details.

Specimen	Shear span ratio	Number of steel plates	Axial force ratio	CFST column type	Retrofitting
S0N1	1.5	0	0.15	Square column	–
S2N1		2	0.15	Square column	
S3N1		3	0.15	Square column	
S3H1		3	0.25	Square column	
S4N1		4	0.15	Square column	
S5N1		Entire plate	0.15	Square column	
C3N1		3	0.15	Circular column	
S0N2R	1.5	0	0.15	Square column	Yes
S2N2R		2	0.15	Square column	Yes
S3N2		3	0.15	Square column	No
S3H2R		3	0.25	Square column	Yes
S4N2R		4	0.15	Square column	Yes
S5N2R		Entire plate	0.15	Square column	Yes
C3N2		3	0.15	Circular column	No

compressive strength used in the test was 34.4 N/mm^2.

$$f_c' = (0.66 + 0.002 f_{cu}^{150}) f_{cu}^{150} \geqslant 0.76 f_{cu}^{150} \quad (2)$$

In the evaluation of the compressive strength, for the square CFST column, the confining effect provided by the square steel tube was small, hence the confining effect is not considered according to Ref. [15]. However, for the circular CFST column, the confining effect was considered due to the high confinement provided by the circular steel tube. The confined concrete strength f_{cc}' was calculated as follows [15]:

$$f_{cc}' = f_c' + 0.78 \cdot \frac{2t}{D-2t} \cdot f_y \quad (3)$$

where t is the wall thickness of steel tube; D is the steel tube diameter; f_y is the steel tube yield strength.

2.2.2. Steel

The steel tube had a strength grade of Q345 (nominal yield strength f_y = 345 N/mm^2), while the multiple steel plates and retrofitting steel plate had a strength grade of Q235 (nominal yield strength f_y = 235 N/mm^2) in the Chinese code [16]. The material properties of the steel were measured by coupon tests, resulting Young's modulus (E_s), yield strengths (f_y) and ultimate strengths (f_u) are shown in Table 2.

In the design of the composite shear walls, the area ratio of the steel plates and steel tubes are key issues. Area ratio of the steel plates is defined as the cross sectional area of the embedded steel plates to the RC walls. Note that when calculating the cross sectional areas of the multiple steel plates, the multiple plates were converted to a single full-size steel plate of equivalent volume. The area ratio of the embedded steel plates of specimen S0N1, S2N1, S3N1, S3H1, C3H1, S4N1 and S5N1, were 0, 0.01, 0.014, 0.014, 0.015, 0.019 and 0.029, respectively. The width-to-thickness (B/t) ratio and the diameter-to-thickness (D/t) ratio of the steel tubes were 35 and 32, respectively. The limitation of the B/t and D/t in the Eurocode 4 [17] and JGJ 138 [18] are listed below:

For Eurocode 4:

$$\text{Square CFST:} \quad \frac{B}{t} \leqslant 52\sqrt{\frac{235}{f_y}} \quad (4)$$

$$\text{Circular CFST:} \quad \frac{D}{t} \leqslant 90 \cdot \frac{235}{f_y} \quad (5)$$

For JGJ 138:

$$\text{Square CFST:} \quad \frac{B}{t} \leqslant 60\sqrt{\frac{235}{f_y}} \quad (6)$$

$$\text{Circular CFST:} \quad \frac{D}{t} \leqslant 135 \cdot \frac{235}{f_y} \quad (7)$$

when f_y = 345 N/mm^2, all specimens can meet the requirements of the design codes mentioned above.

2.3. Test setup and measurements

Loading program: As shown in Fig. 3, the foundation beam of the specimen was firmly clamped to the reaction floor. The loading beam was connected to a vertical and a horizontal hydraulic jack. First, the target vertical load was generated by the vertical jack. After that, the cyclic lateral loads were applied quasi-statically to the loading beam. The vertical load was kept constant throughout the entire test.

Two loading stages were applied to all specimens, as follows.

Stage 1: During this stage, as shown in Fig. 4(a), the loading program was determined by the Chinese specification [19], that is before the yielding of the specimen, loading process was in load-controlled mode. After the yielding of the specimen, the loading process was controlled by the horizontal displacement. The specimens were tested until a 2.0% drift ratio was reached. In the discussions presented later in this paper, the drift ratio θ rather than the horizontal displacement Δ is used, this is because the displacement Δ depends on the height of the specimen as well. The drift ratio θ is defined as $\theta = \Delta/H$, where Δ is the horizontal displacement, and H is the height from the loading point to the wall base, as shown in Fig. 5. In the seismic design code of buildings in China [4], the limitation of the elastic-plastic displacement angle of the shear wall is taken as 1/120, which is much smaller than 2.0%. Fig. 6(a) shows a photograph of the specimen during stage 1.

Stage 2: After stage 1, specimens S0N1, S2N1, S4N1, S5N1 and S3H1 were retrofitted by welding a 2 mm thick steel plate on either side of the shear walls. Fig. 6(b) shows a photograph of a retrofitted specimen during stage 2. Specimens S3N1 and C3N1 were not retrofitted to determine the effects of the retrofitting work. During stage 2, the loading process was controlled by the horizontal displacement from the beginning, as shown in Fig. 4(b). During this stage, all retrofitted and un-retrofitted specimens were tested after the loading was decreased below 85% of the maximum load.

Measurements: The loads, displacements and strains were measured during the test. Load cells were used to measure the vertical load and the horizontal forces applied to the specimens. The LVDTs were used to measure the displacement of the specimens. The layout of the LVDTs is shown in Fig. 3. Two LVDTs were used to measure the horizontal displacements at the loading beam, 1100 mm from the surface of the foundation. Two LVDTs were placed on the foundation to monitor the slippage and lean of the foundation. The strain gauges were used at the top and bottom of the steel tube, the multiple steel plates, the retrofitted steel plate and the vertical reinforcing bars.

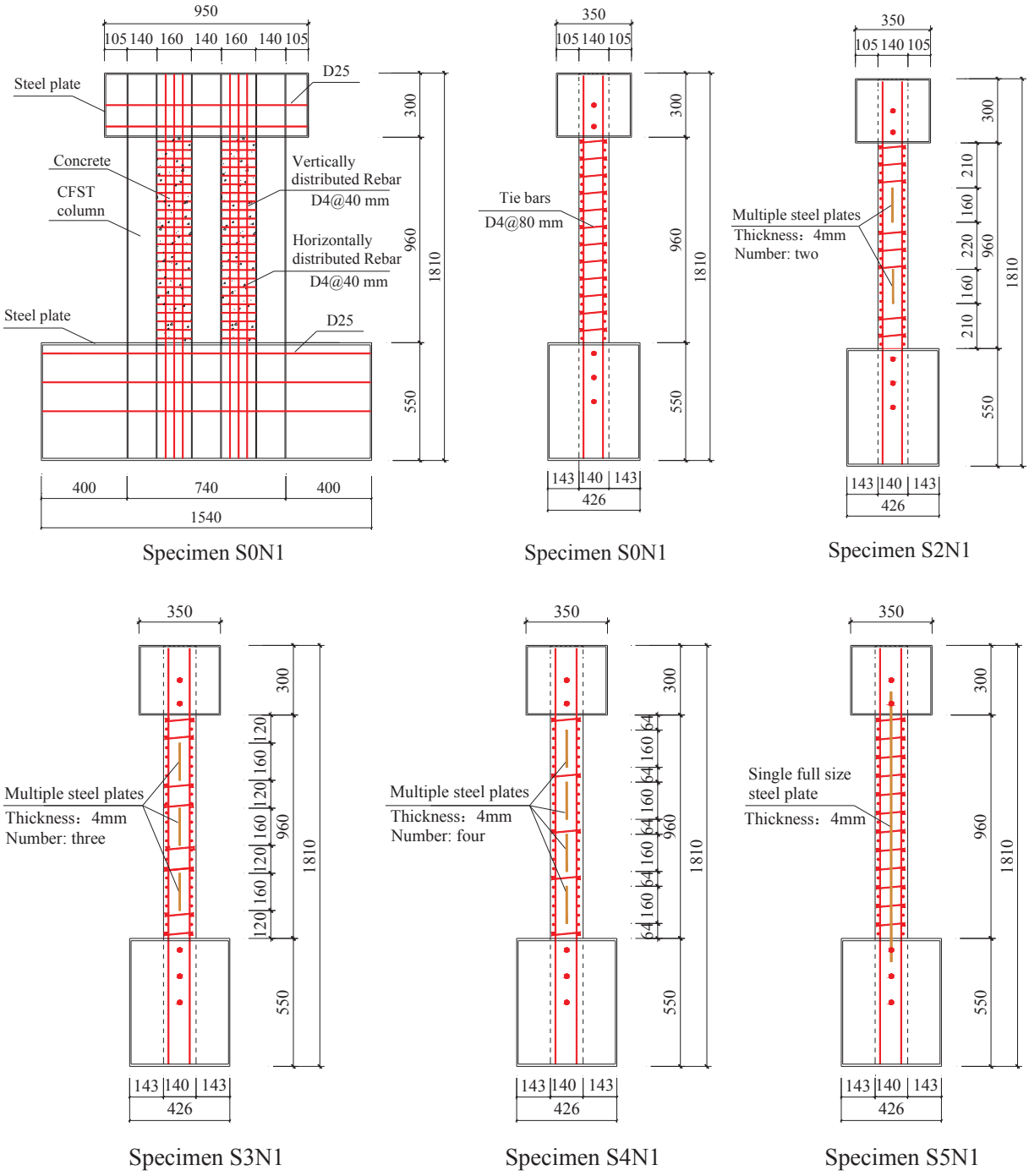

(a) Elevation drawings of specimens

Fig. 2. Specimen details (units: mm).

3. Test results and discussions

3.1. Damage and failure characteristics

3.1.1. Stage 1

Fig. 7(a)–(e) shows the overall damage and failure characteristics of specimens S0N1, S2N1, S3N1, S4N1 and S5N1. Initial diagonal cracks were observed on the bottom part of the shear wall under normal axial force ratio at approximately 0.16% drift ratio. The initial cracks on specimen S3H1 with higher axial force ratio appeared at 0.18% drift ratio, which was a little later than in the other specimens.

During the early loading period, small cracks were also found at the interface of the CFST columns and the RC walls. As the loading proceeded, these small cracks turned into damage zones, which are marked with red circles in Fig. 7(a)–(e). However, as the number of multiple steel plates increased, the damage zones became smaller, indicating that the embedded multiple steel plates have an effect on the reduction of the damages at the interface of the CFST columns and the RC walls. This is also an indication that the multiple steel plates had an important effect on the energy dissipation during the damage process. During this

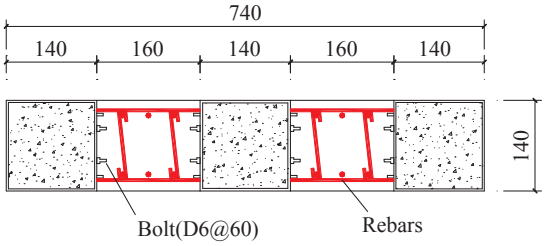

Specimen S0N1

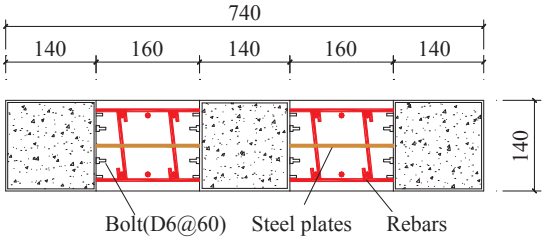

Specimens S2N1, S3N1, S3H1, S4N1, S5N1

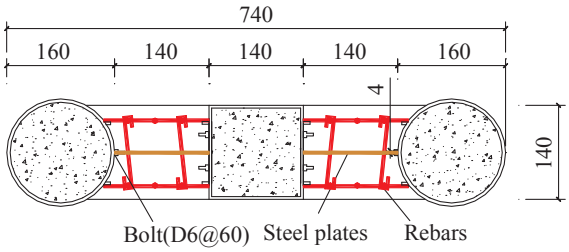

Specimen C3N1

(b) Cross section of specimens

(c) Core steel structures of the specimens

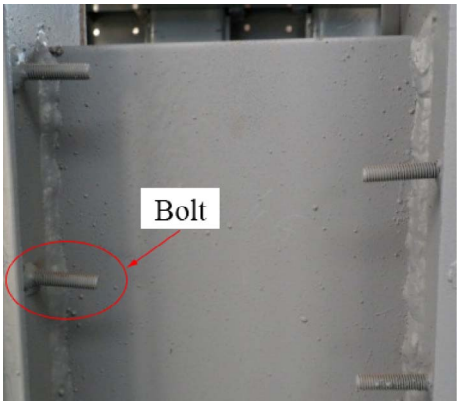

(d) Bolts along the steel tubes-concrete interface

Fig. 2. (*continued*)

Table 2
Mechanical properties of steel materials.

Steel type	f_y (MPa)	f_u (MPa)	E_s (MPa)
140 mm × 4 mm square tube	375	508	2.05×10^5
160 mm × 5 mm circular tube	380	510	2.04×10^5
Steel plates (4 mm thickness)	270	401	2.06×10^5
Retrofitting steel plate (2 mm thickness)	252	389	2.05×10^5
D4 reinforcing bar	634	738	2.06×10^5

stage, slight local buckling of the square steel tube was observed, as shown in Fig. 7(f). No obvious local buckling was confirmed for the circular steel tube.

3.1.2. Stage 2

The failure characteristics of the specimens after stage 2 are shown in Fig. 8. The damage progression and the failure characteristics are analyzed as follows:

Fig. 8(a)–(d) shows the failure characteristics of retrofitted specimens S0N2R, S2N2R, S4N2R and S5N2R after stage 2. For specimens S0N2R and S2N2R, when the drift ratio θ reached approximately 1/80, a diagonal tension strip was formed on the steel plate. When the drift ratio θ reached approximately 1/50, the diagonal tension strip became

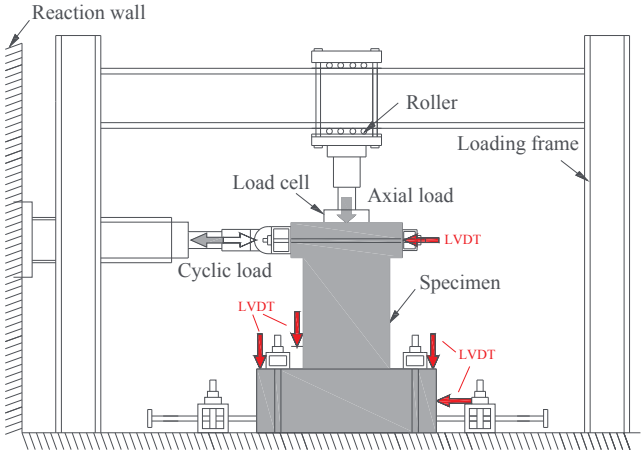

Fig. 3. Test setup.

more evidently, and the retrofitting steel plate yielded considerably. However, increasing the number of multiple steel plates reduced the diagonal tension strip on the retrofitting steel plate, this trend can be confirmed on Fig. 8(a) to (d). Especially for specimen S5N1 with the

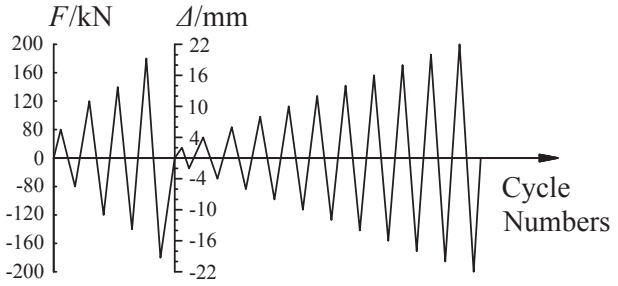

(a) Loading stage 1

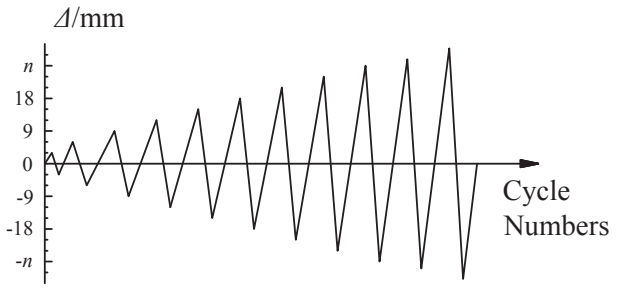

(b) Loading stage 2

Fig. 4. Loading program.

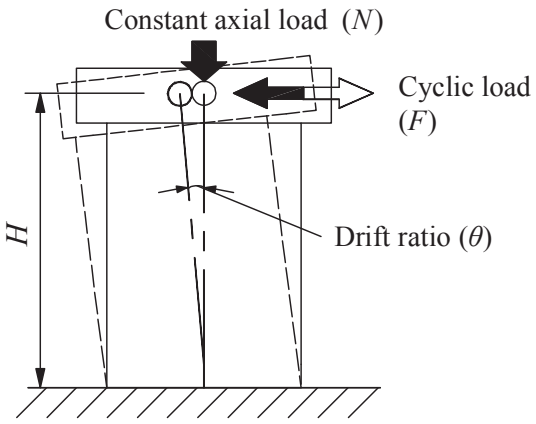

Fig. 5. Definition of drift ratio θ.

embedded single full-size steel plate, almost no diagonal tension strips were observed. It is observed that as the number of embedded multiple steel plates increases, the effect of the retrofitting steel plate decreases.

The damages on un-retrofitted specimens S3N2 and C3N2 were more serious than those on the retrofitted specimens. The overall failure characteristic of specimen S3N2 is shown in Fig. 8(e). The failure characteristics observed confirmed that the retrofitting method can have a positive effect on reducing the damages of the specimens.

Compared to specimens in stage 1, the steel tubes in stage 2 experienced more serious damage. Fig. 8(f) shows the typical failure characteristics of square CFST column specimens, where vertical fracture and concrete crushing were observed. Local buckling and horizontal fracture were also found on the circular steel tube of specimen C3N2, shown in Fig. 8(g).

3.2. Hysteretic behavior

The relationships between the horizontal force F and the drift ratio θ of all specimens under both loading stages are shown in Fig. 9. In the figures, the hysteretic curves in black represent the results obtained during stage 1. During this stage, the drift ratio was controlled until 2.0%. The red curves in the figures are the skeleton curves of the specimens during stage 2. Note that, to simplify the figures, the skeleton curves but not the hysteretic curves were adopted to describe the results of stage 2. Table 3 shows all characteristic loads, such as the cracking strength, F_c, the cracking drift ratio, θ_c, the yield load, F_y, the yield drift ratio, θ_y, the maximum strength, F_m, the maximum drift ratio, θ_m, the ultimate strength, F_u, and the ultimate drift ratio, θ_u. Where, the crack load, F_c, was determined as the load registered when initial cracking occurred. The yield load, F_y, was determined by the energy equivalent method [20], as shown in Fig. 10. The ultimate load, F_u, was the load corresponding to 85% of the maximum load, F_m.

3.2.1. Stage 1

During this stage, all the hysteretic curves were stable, showing good seismic behavior. No obvious strength deterioration occurred during stage 1. However, the strength of specimen S0N1, with no multiple steel plates, was considerably smaller than that of other specimens, indicating the strength enhancement obtained with the use of embedded multiple steel plates. During the test, when the drift ratio was small (i.e. $\theta < 1/400$), there was no observable residual deformation. However, when the drift ratio θ was greater than 1/250, there was an observable residual deformation. The parametrical studies are as follows:

(1) *Effect of the number of multiple steel plates*

Fig. 11(a) shows a comparison of the skeleton curves of the specimens with different number of multiple steel plates during stage 1. With an increasing number of multiple steel plates, the strength at 2.0% drift ratio also increased. For specimens S2N1, S3N1, S4N1 and S5N1, the strengths were, respectively, 1.25, 1.35, 1.35 and 1.52 times larger than that of specimen S0N1. As shown in Fig. 11(b), the results show that the embedded multiple steel plates were able to improve the strength of the specimens. In Fig. 11(b), the horizontal axis indicates the total height h of the multiple steel plates, while the vertical axis shows the strength at 2.0% drift ratio. As shown, the height h of the steel plate for specimen S5N1 was 960 mm, while for specimen S3N1 it was 480 mm. In other words, the amount of steel used in specimen S5N1 was 2.00 times larger than that in S3N1. However, the strength at 2.0% drift ratio of specimen S5N1 was only 1.12 times higher than that of specimen S3N1. The strength did not increase proportionally to the amount of embedded multiple steel plates. The optimal number of embedded multiple steel plates should be considered in the seismic design of the developed shear walls. For the limited configurations considered in this study, the specimen with three multiple steel plates was the most cost effective.

(2) *Effect of boundary CFST columns*

Specimens S3N1 and C3N1 consist of square and circular CFST columns, respectively. Fig. 12 shows a comparison of the skeleton curves of the two specimens. As shown in Table 3 and Fig. 12, the maximum strength of circular column specimen C3N1 was 1.10 times greater than that of square column specimen S3N1. This is because of two reasons. The first reason is the circular CFST column experienced better confinement than the square one, thus the strength of the concrete inside the circular tube was greater. The second reason is the cross sectional area of the circular CFST was higher than that of the square CFST. However, specimens with square or circular boundary CFST columns had stable hysteresis, which satisfy the needs of different engineering projects.

(3) *Effect of axial force ratio*

The axial force ratios of specimens S3N1 and S3H1 were 0.15 and 0.25, respectively. The yield and ultimate strength of specimen S3H1

(a)Specimen under stage 1 loading (b) Specimen after retrofitting

Fig. 6. Photographs of specimens.

were 1.05 and 1.03 times greater than that of specimen S3N1, respectively. This is because when the axial force ratio increased, the contribution to the bending moment of the concrete part also increased.

3.2.2. Stage 2

Effects of retrofitting work are discussed in the following.

(1) *Stiffness*

As shown in Fig. 9, during stage 2, the stiffness of un-retrofitted specimens S3N2 and C3N2 was much smaller than that of specimens S3N1 and C3N1 during stage 1. This was due to accumulated damages on the specimens during stage 1. The stiffness of retrofitted specimens S0N2R, S2N2R, S3H2R and S4N2R with embedded multiple steel plates only decreased slightly compared to the corresponding stiffness during stage 1. It is indicated that the retrofitting steel plate can enhance the stiffness of the damaged shear walls. However, for retrofitted specimen S5N2R with an embedded full-size steel plate, stiffness decreased a lot more.

(2) *Strength*

Fig. 13 shows the effect of the retrofitting work on strength. The vertical axis is defined as N_2/N_1, where N_2 is the strength during stage 2 at 2.0% drift ratio, N_1 is the strength during stage 1 at 2.0% drift ratio. For un-retrofitted specimen S3N1, the strength during stage 2 was slightly smaller than that during stage 1, the value of N_2/N_1 was 0.96. The values of N_2/N_1 of retrofitted specimens S0N2R, S2N2R, S4N2R and S5N2R were 1.51, 1.27, 1.14 and 1.04, respectively. Although the strength increased with increasing number of multiple steel plates, the difference between the two stages decreased. The retrofitting steel plate was shown to cause an increase in the strength of the shear walls. However, the retrofitting showed almost no effect on specimen S5N2R. This was confirmed and discussed in the failure characteristics in Section 3.1 and can be explained as follows: Specimen S5N1 already had high shear resistance capacity due to the embedded full-size continuous steel plate. Hence, the retrofitting method, which intended to increase shear resistance capacity, showed almost no effect on the specimen. The reasonable retrofitting method for specimen S5N1 should be the strengthening of the plastic hinges at the boundary CFST column bases to enhance the bending resistance capacity of the shear wall. In the retrofitting design, different retrofitting methods should be taken into account according to the different types of the shear wall.

(3) *Ductility*

Displacement ductility ratio μ was defined as $\mu = \theta_u/\theta_y$ [21,22]. Fig. 14 shows the ductility ratio of the specimens during stage 2. As shown, ductility ratios of retrofitted specimens S2N2R, S4N2R and S3H2R with embedded multiple steel plates were 2.16, 2.32 and 2.27, respectively. The average ductility ratio was 2.25. On the other hand, ductility ratios of un-retrofitted specimens S3N2 and C3N2 were 1.82 and 1.71, with an average value of 1.77. These results confirm that the retrofitting method had an evident effect on improving the ductility of the shear walls with embedded multiple steel plates.

3.3. Behavior of embedded multiple steel plates

Typical strain characteristics of specimen S3N1 during stage 1 are shown in Fig. 15. Strain gauges were used at three locations to measure the behavior of the embedded multiple steel plates. At each location, the strain gauges were attached to both sides of the embedded multiple steel plates. Fig. 15 shows the results of the gauges in the middle plate. As shown, the multiple steel plates reached the yield strain around 0.8% drift ratio. The strain gauges in the front and back of the plates yielded almost identical results, indicating that at 2.0% drift ratio, no local buckling is found from the strain gauge results i.e. at the location of strain gauges due to the strong restraint provided by the RC concrete.

3.4. Energy dissipation capacity

The energy dissipation capacities of the seven specimens during stages 1 and 2 are shown in Fig. 16. The energy dissipation capacity, E_p, is defined as the area enclosed by the skeleton curves at 2.0% during stage 1 or 2. The following observations are made:

(1) *Stage 1*

For specimens S0N1, S2N1, S3N1, S4N1 and S5N1, increasing the number of the multiple steel plates caused the energy dissipation

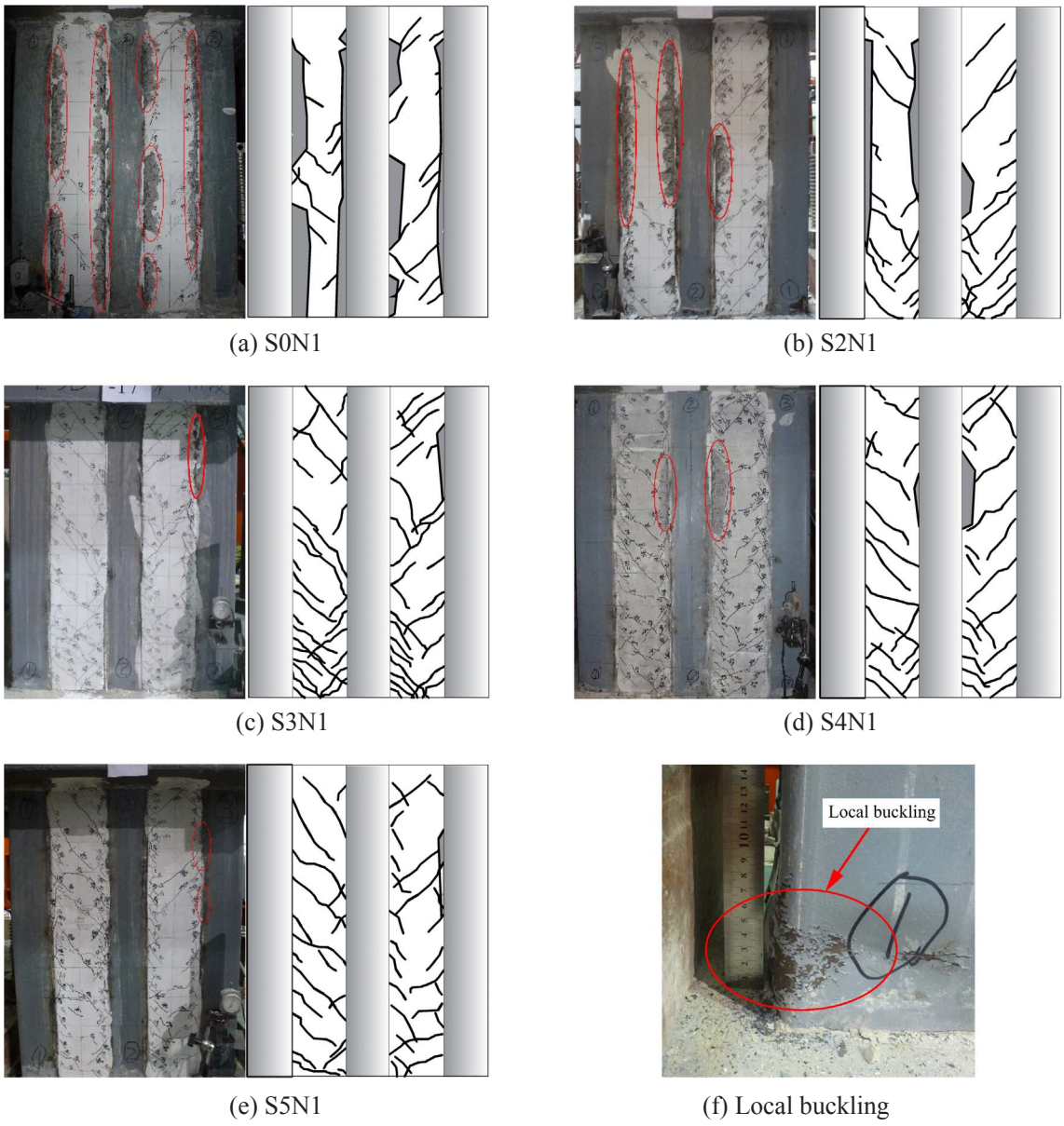

Fig. 7. Failure characteristics of specimens after stage 1.

capacity to initially increase and then decrease. Specimen S3N1 with three embedded multiple steel plates had the largest energy dissipation capacity. It was 29% larger than that of specimen S5N1 which has the single full-size steel plate. This may be due to the fact that the upper part of the single full-size steel plate did not yield according to the results of the strain gauges shown in Fig. 17. However, the multiple steel plates of all innovative specimens yielded according to the results of the strain gauges. For this reason, in the seismic design of innovative shear walls, it does not mean the more embedded multiple steel plates, the better energy dissipation capacity. The amount of multiple steel plates should be matched to the capacity of the boundary CFST columns and RC walls. In accordance with this study, the innovative shear walls with three embedded multiple steel plates had a better energy dissipation capacity than the other configurations considered.

Specimens S3N1 and C3N1 have different types of CFST columns. As shown in Fig. 16, the energy dissipation capacity of Specimen C3N1 was 20% higher than that of specimen S3N1. This is because the circular CFST column had higher strength and ductility.

When observing the effect of axial force ratio, it is confirmed that the higher the axial force ratio, the better energy dissipation capacity. This is because the strength was greater for specimen S3H1 which had a higher axial force ratio.

(2) *Stage 2*

As shown in Fig. 16, the energy dissipation capacity of four retrofitted specimens: S0N2R, S2N2R, S4N2R and S5N2R first increased then decreased during the stage 2. The energy dissipation capacity of specimen S5N2R with a single full-size steel plate was small. This is because the effect of the retrofit on specimen S5N2R was not considerable, which was confirmed in Sections 3.1 and 3.2. The energy dissipation capacity of un-retrofitted specimen S3N2 was 29.5% lower than that of specimen S3N1 during stage 1. It is indicated that the energy dissipation capacity of specimens decreased with increased loading cycles. However, the energy dissipation of un-retrofitted specimen S3N2 (i.e. $E_p = 10.3$) was still higher than that of retrofitted specimens S0N2R (i.e. $E_p = 10.1$) and S5N2R (i.e. $E_p = 9.5$). The specimen with three steel plates was proven to have excellent energy dissipation capacity compared with other specimens.

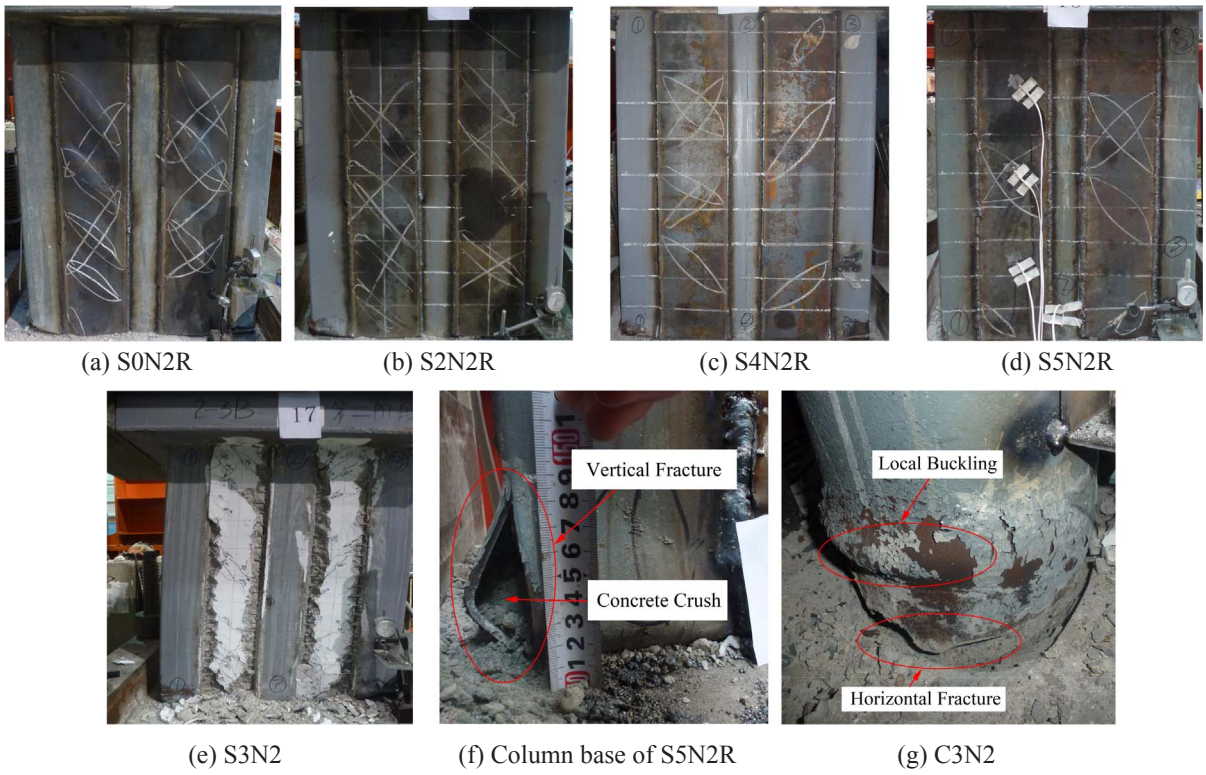

(a) S0N2R (b) S2N2R (c) S4N2R (d) S5N2R

(e) S3N2 (f) Column base of S5N2R (g) C3N2

Fig. 8. Failure characteristics of specimens after stage 2.

3.5. Degradation of stiffness

Table 4 shows the experimental results of the average secant stiffness of specimens with different multiple steel plates during stage 1. Fig. 18 shows the average secant stiffness at different drift ratios. The average secant stiffness of the test specimens is defined as:

$$K_i = \frac{(F_i^+/\Delta_i^+ + F_i^-/\Delta_i^-)}{2} \tag{8}$$

where K_i is the average specimen stiffness when it is subjected to the negative and positive loads of the ith cycle; F_i^+ and F_i^- are the maximum positive and negative loads of the ith cycle, respectively; while Δ_i^+ and Δ_i^- are the maximum drift ratios resulting from the positive and negative loads of the ith cycle, respectively. In Fig. 18, K_0 represents the initial stiffness.

The following observations are obtained from Fig. 18 and Table 4.

(1) *Stage 1*

In general, the degradation of stiffness can be roughly divided into three phases. The first phase is the fast degradation phase, which starts from the beginning of the loading to the appearance of the first crack. The second phase presents relatively fast degradation. It starts with the appearance of the first crack and ends with the yielding of the specimens. The third phase is the slow degradation phase, which starts with the yielding of the specimens and lasts until the end of the experiment.

The stiffness at the crack point, K_c, of specimens S0N1, S2N1, S3N1, S4N1 and S5N1 ranged from 71.6 to 75.7 kN/mm, and no obvious difference was observed. The stiffness at the yield point, K_y, of specimens S2N1, S3N1, S4N1 and S5N1was, respectively, 6%, 11%,3% and 16% higher than that of specimen S0N1, while the stiffness at the maximum point, K_m, was, respectively, 25%, 35%, 35% and 52% higher than that of specimen S0N1. These results indicate that the stiffness increases with an increasing number of multiple steel plates. Specimen S3N1 with three multiple steel plates exhibited slower degradation of the average secant stiffness.

(2) *Stage 2*

For retrofitted specimens S0N2R, S2N2R, S4N2R and S5N2R, the stiffness at the yield point, K_y, ranged from 25.1 to 32.0 kN/mm (the average value was 29.6 kN/mm), the stiffness at the maximum point, K_m, ranged from 17.0 to 22.1 kN/mm (the average value was 19.8 kN/mm), the stiffness at the ultimate point, K_u, ranged from 12.1 to 14.6 kN/mm (the average value was 13.2 kN/mm). For un-retrofitted specimen S3N2, the stiffness at the yield point, the maximum point and the ultimate point was 21.1, 16.2 and 9.3 kN/mm, respectively. It is confirmed that the stiffness of un-retrofitted specimens was much lower than that of retrofitted specimens, hence, the retrofitting method can considerably enhance the stiffness of the specimens.

4. Evaluation for ultimate strength

4.1. Evaluation model for strength

An evaluation model for the innovative composite shear walls was developed, as shown in Fig. 19. In this Figure, F is the horizontal load; N is the axial load; N_1, N_2, and N_3 represent the axial load distributed among the columns; F_1, F_2, and F_3 represent the distribution of the lateral load to the columns; V_i is the shear force provided by the ith plate; V_{RC} is the shear force provided by the RC walls. The assumptions made in the development of the evaluation model are: (1) Expect the lateral and vertical translation at the top, other degrees of freedom at the top and bottom of the composite columns are restrained. (2) The vertical load is equally distributed among the CFST columns. (3) Full plastic behavior of the materials is considered. (4) Tensile strength of concrete is considered negligible.

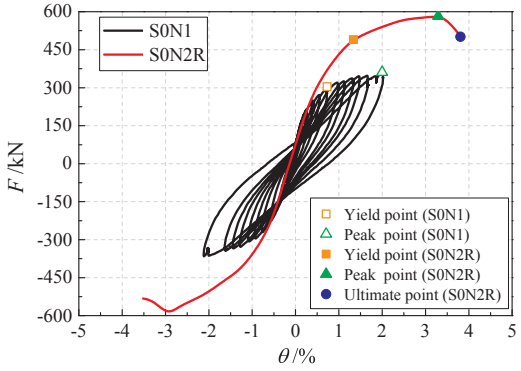

(a) S0N1, S0N2R

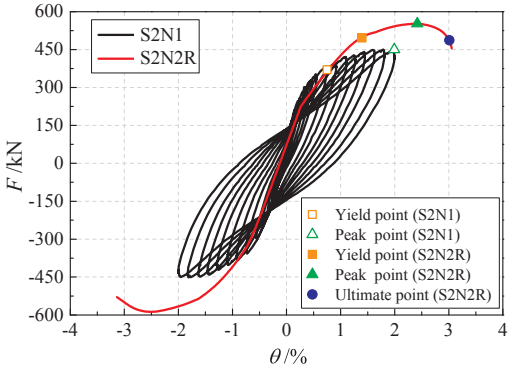

(b) S2N1, S2N2R

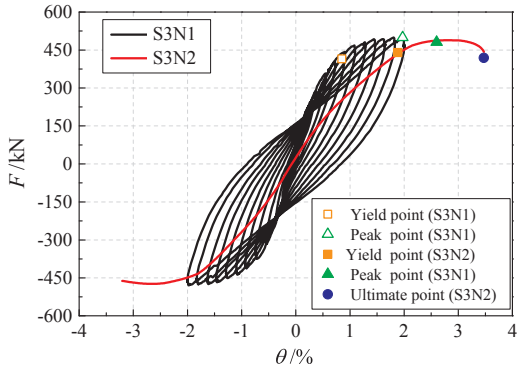

(c) S3N1, S3N2

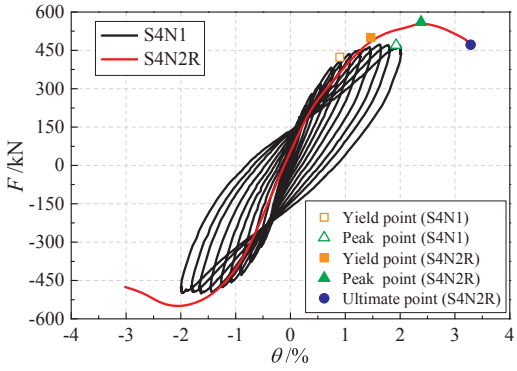

(d) S4N1,S4N2R

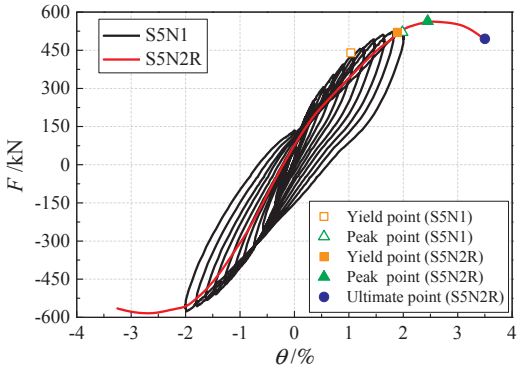

(e) S5N1,S5N2R

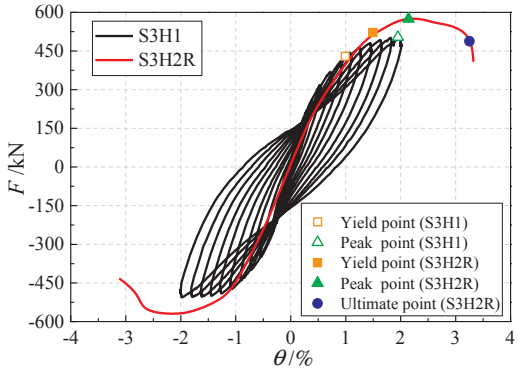

(f) S3H1, S3H2R

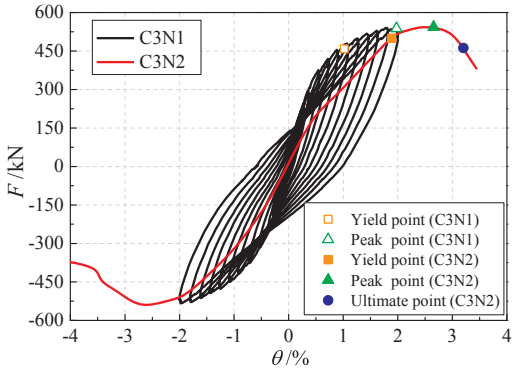

(e) C3N1, C3N2

Fig. 9. Hysteretic curves and skeleton curves during loading stages 1 and 2.

Table 3
Summary of specimens' strengths and deformations.

Test period	Specimen	Crack		Yield		Maximum		Ultimate	
		F_c (kN)	θ_c (rad)	F_y (kN)	θ_y (rad)	F_m (kN)	θ_m (rad)	F_u (kN)	θ_u (rad)
Stage 1	S0N1	120	1/669	304	1/137	361	1/50	–	–
	S2N1	125	1/645	352	1/125	450	1/50	–	–
	S3N1	126	1/630	409	1/113	489	1/50	–	–
	S4N1	130	1/617	423	1/111	487	1/50	–	–
	S5N1	140	1/600	499	1/97	549	1/50	–	–
	S3H1	148	1/560	430	1/107	504	1/50	–	–
	C3N1	131	1/623	459	1/98	538	1/50	–	–
Stage 2	S0N2R	–	–	455	1/74	589	1/32	501	1/27
	S2N2R	–	–	496	1/72	573	1/38	487	1/31
	S3N2	–	–	440	1/53	485	1/37	412	1/29
	S4N2R	–	–	507	1/68	556	1/44	472	1/30
	S5N2R	–	–	528	1/53	576	1/39	489	1/28
	S3H2R	–	–	522	1/69	574	1/47	488	1/30
	C3N2	–	–	500	1/53	544	1/38	462	1/31

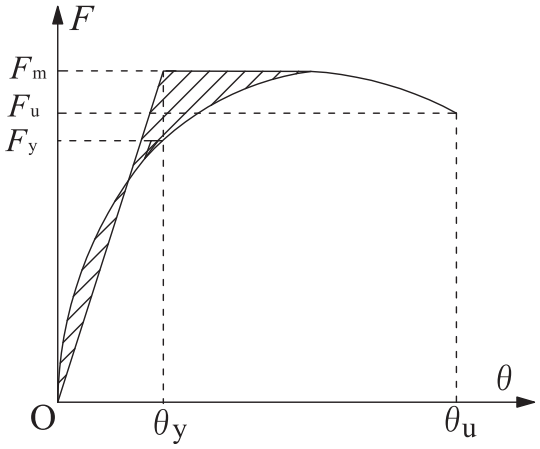

Fig. 10. Definition of F_y, F_m and F_u.

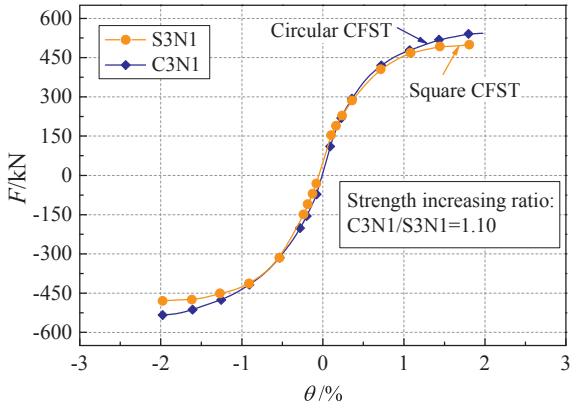

Fig. 12. Effect of concealed composite columns.

4.2. Evaluation formulas for strength

According to the moment equilibrium, the following equations were established:

(1) *Calculation of ultimate strength on left column 1*

$$F_1 = \frac{M_1 + M_1' + V_{RC}\cdot b/2 + \sum_{i=1}^{n} V_i\cdot(L+b)/2}{H} \tag{9}$$

(2) *Calculation of ultimate strength on middle column 2*

$$F_2 = \frac{M_2 + M_2' + V_{RC}\cdot b + \sum_{i=1}^{n} V_i\cdot(L+b)}{H} \tag{10}$$

(3) *Calculation of ultimate strength on right column 3*

$$F_3 = \frac{M_3 + M_3' + V_{RC}\cdot b/2 + \sum_{i=1}^{n} V_i\cdot(L+b)/2}{H} \tag{11}$$

(4) *Calculation of shear strength provided by multiple steel plates*

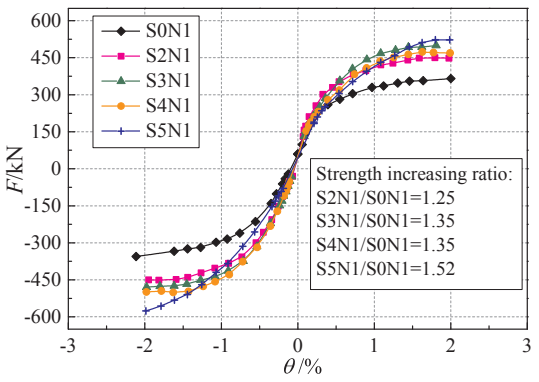

(a) Skeleton curves

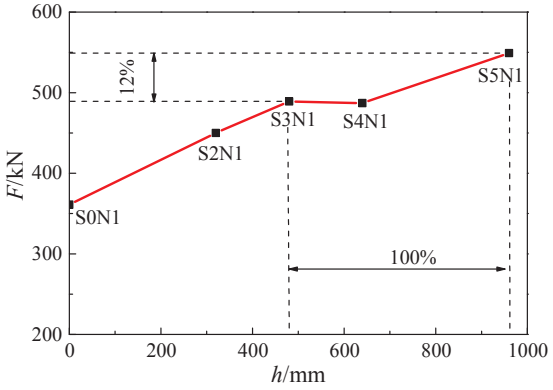

(b) Effects of the number of steel plates on strength

Fig. 11. Effect of the number of steel plates on specimens' strength.

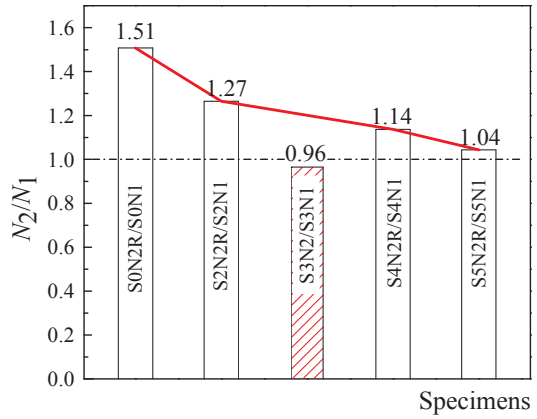

Fig. 13. Effect of retrofitting steel plate on strength.

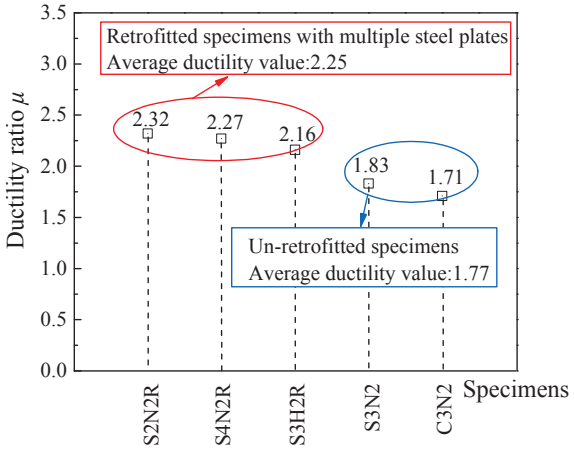

Fig. 14. Ductility ratios.

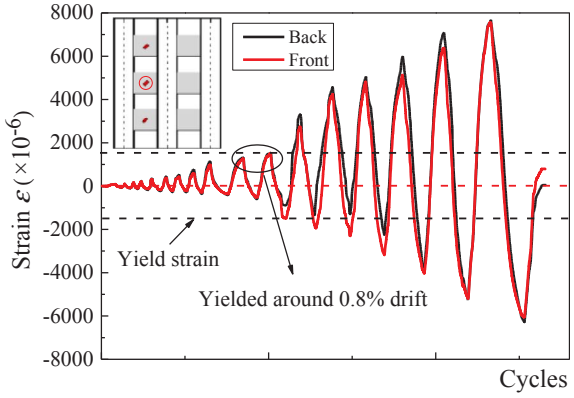

Fig. 15. Strain characteristics of embedded steel plates in Specimen S3N1.

$$V_i = f_{y,sp} h_{sp} t_{sp} \tag{12}$$

(5) *Calculation of shear strength provided by the boundary of the RC wall*

$$V_{RC} = K(V_c + V_s) = K(0.5 f_c' Lw + f_{y,b} A_{s,b}) \tag{13}$$

(6) *Ultimate strength of the shear wall with boundary CFST columns and multiple steel plates*

$$F = F_1 + F_2 + F_3 \tag{14}$$

where b is the width of the CFST column (=140 mm); L is the width of the RC wall (=160 mm); H is the height from the loading point to the foundation surface (=1100 mm); f_{sp} is the yield strength of the steel plate; t_{sp} is the thickness of the steel plate; h_{sp} is the height of the steel plate; V_c is the shear strength provided by the concrete wall; V_s is the shear strength provided by the horizontal reinforcing bars; f_c' is the cylinder compressive strength of concrete; w is the thickness of the concrete wall; $f_{y,b}$ is the yield strength of the horizontal reinforcing bars; $A_{s,b}$ is the sectional area of the horizontal steel bars; K is the contribution factor of the RC wall to the shear strength, taken as 0.6 [12]; M_1, M_2 and M_3 are the moment of the upper part of the left CFST column 1, middle CFST column 2 and right CFST column 3, respectively; M_1', M_2' and M_3' are the ultimate moment of the lower part of the left CFST column 1, middle CFST column 2 and right CFST column 3, respectively.

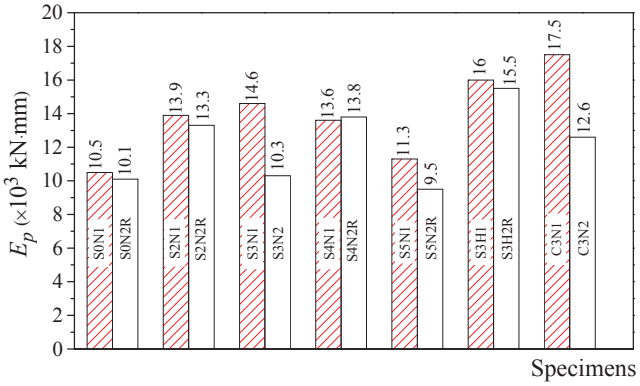

Fig. 16. Energy dissipation under 2.0% drift ratio.

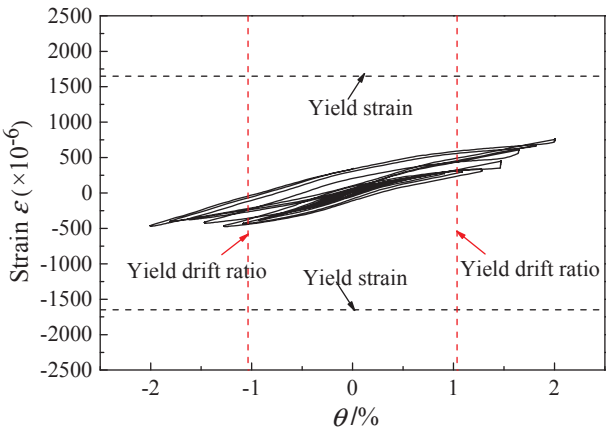

Fig. 17. Strain in the upper part of the steel plate in specimen S5N1.

According to the AIJ [15], the ultimate bending strength M of the square and circular CFST columns are calculated as follows:

$$N = N_c + N_s \tag{15}$$

$$M = M_c + M_s \tag{16}$$

For the square CFST column,

$$N_c = x_n \cdot B_c \cdot f_c' \tag{17}$$

$$M_c = 0.5(B_c - x_n) B_c \cdot x_n \cdot f_c' \tag{18}$$

$$N_s = 2t(2x_n - B_c) f_y \tag{19}$$

$$M_s = Bt(B - t) f_y + 2t(B_c - x_n) x_n \cdot f_y \tag{20}$$

For the circular CFST column,

$$N_c = r_1^2(\alpha - \sin\alpha\cos\alpha) f_{cc}' \tag{21}$$

Table 4
Stiffness experimental results.

Specimen	Crack point		Yield point		Maximum point		Ultimate point	
	K_c (kN/mm)	Relative value	K_y (kN/mm)	Relative value	K_m (kN/mm)	Relative value	K_u (kN/mm)	Relative value
S0N1	72.3	1.00	37.5	1.00	16.4	1.00	–	–
S2N1	72.7	1.01	39.6	1.06	20.5	1.25	–	–
S3N1	71.6	0.99	41.7	1.11	22.2	1.35	–	–
S4N1	72.2	1.00	42.3	1.13	22.1	1.35	–	–
S5N1	75.7	1.05	43.4	1.16	25.0	1.52	–	–
S0N2R	–	–	30.1	1.00	17.0	1.00	12.1	1.00
S2N2R	–	–	32.0	1.06	19.8	1.16	14.6	1.21
S3N2	–	–	21.1	0.70	16.2	0.95	9.3	0.77
S4N2R	–	–	31.1	1.03	22.1	1.30	12.9	1.07
S5N2R	–	–	25.1	0.83	20.2	1.19	13.0	1.08

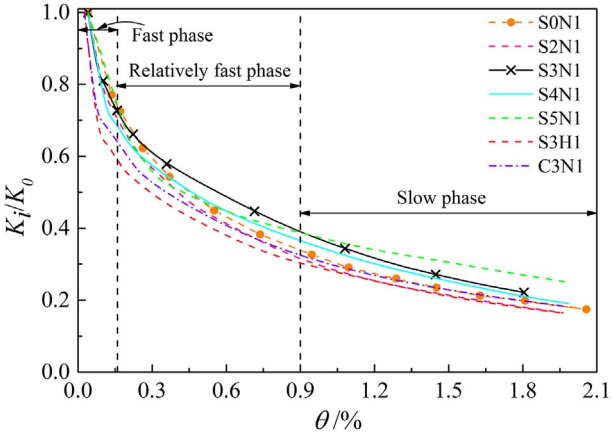

Fig. 18. Stiffness ratio at different drift ratios.

$$M_c = \frac{2}{3} r_1^3 \sin^3\alpha \cdot f'_{cc} \tag{22}$$

$$N_s = 2r_2 t\{\beta_1\alpha - \beta_2(\alpha-\pi)\}f_y \tag{23}$$

$$M_s = 2r_2^2 t(\beta_1 - \beta_2)\sin\theta \cdot f_y \tag{24}$$

where N is the axial force of the CFST column; N_c is the axial force of the concrete; N_s is the axial force of the steel tube; M_c is the bending moment provided by the concrete; M_s is the bending moment provided by the steel tube; x_n is the neutral axis; f_c' is the cylinder compressive

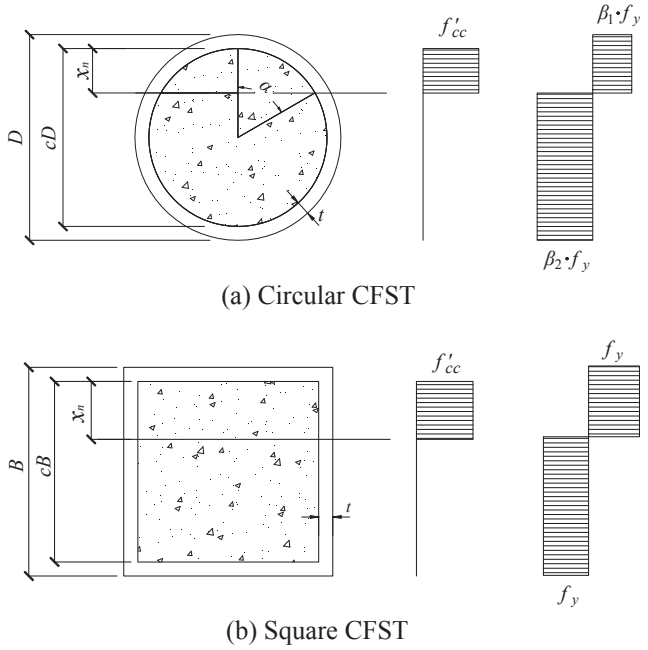

Fig. 20. Stress distribution of the CFST columns for the ultimate strength.

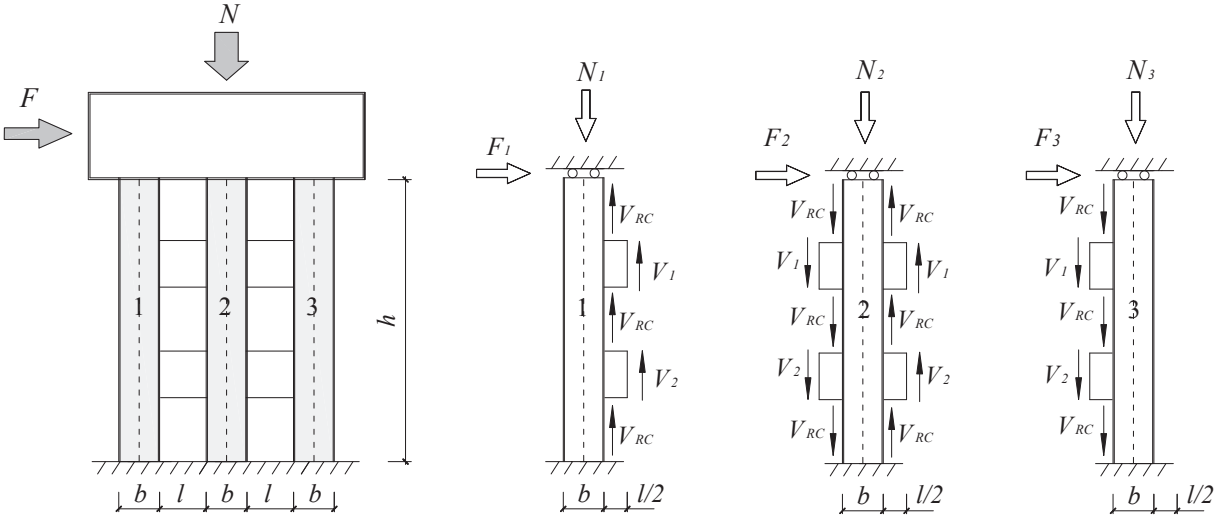

Fig. 19. Evaluation model of shear walls.

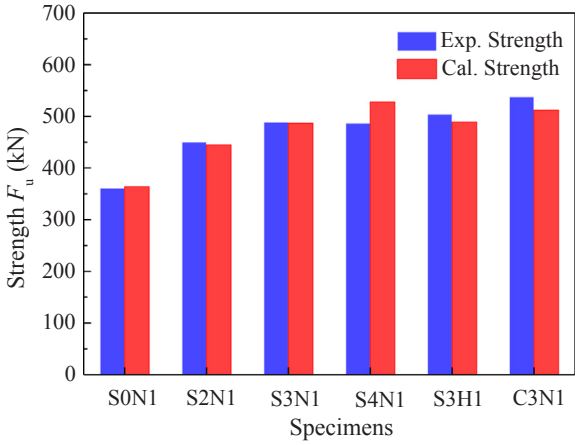

Fig. 21. Calculated and experimental strengths.

strength of concrete; f_{cc}' is the compressive strength of concrete considering the confining effect, which is calculated according to Eq. (3); f_y is the yield strength of the steel tube; t is the thickness of the steel tube; B is the width of the square steel tube; B_c is the width of the square infilled concrete.

$$r_1 = \frac{{}_cD}{2},\ r_2 = \frac{D-t}{2},\ \alpha = \cos^{-1}(1-2x_n/{}_cD),\ \beta_1 = 0.89,\ \beta_2 = -1.08$$

D is the diameter of the circular steel tube; D_c is the diameter of the circular infilled concrete. α is the angle shown in Fig. 20(a), β_1 and β_2 are the coefficients of the stress block shown in Fig. 20(a).

Fig. 21 compares the calculated strengths F_u based on the proposed method to the experimental values obtained. It is confirmed that the evaluation method for ultimate strength had an adequate accuracy.

5. Conclusions

An innovative composite shear wall composed of boundary CFST columns, embedded multiple steel plates, and RC walls has been developed. A total of seven specimens were designed and fabricated. Cyclic loading tests under two loading stages were carried out. Based on this study, the main conclusions are:

(1) The developed innovative composite shear walls with multiple steel plates had stable hysteretic curves.
(2) The number of embedded multiple steel plates considerably affected the seismic behavior of the shear wall. Specimen S3N1 with three multiple steel plates was the most cost-effective with respect to seismic behavior.
(3) The effect of the two types of boundary CFST columns considered, square and circular on the seismic behavior of the wall were similar. Both types of boundary CFST columns can be used to suit the construction needs.
(4) Retrofitting of the innovative shear walls was conducted after the first stage of loading and it considerably enhanced the behavior of the damaged walls. However, designers of the retrofit should assure that the strength of the retrofitting steel plate matches the strength of the shear wall.
(5) An evaluation method for the ultimate strength of the proposed shear wall was developed. This method showed an adequate accuracy in the evaluation of the ultimate strength.

The present paper revealed the advantages and behaviors of the developed shear walls with multiple steel plates subjected to cyclic tests. However, more experimental and analytical studies are needed to develop design provisions and theoretical models for such walls.

Acknowledgements

This work was supported by a National Natural Science Foundation of China grant funded by the Chinese government (No. 51408017). The support is greatly appreciated.

References

[1] Bekő A, Rosko P, Wenzel H, et al. RC shear walls: full-scale cyclic test, insights and derived analytical model. Eng Struct 2015;102:120–31.
[2] Lestuzzi P, Bachmann H. Displacement ductility and energy assessment from shaking table tests on RC structural walls. Eng Struct 2007;29(8):1708–21.
[3] CEN. Eurocode 8: design provisions for earthquake resistance-part 1: general rules∗ seismic actions and rules for buildings. Bruxelles: European Committee for Standardization; 2004.
[4] CMC. Code for seismic design of buildings (GB 50011-2010). Beijing: China Ministry of Construction; 2010. [in Chinese].
[5] ACI. Building code requirements for structural concrete and commentary (ACI 318-08). Farmington Hills: American Concrete Institute; 2008.
[6] Wang B, Jiang HJ, Lu XL. Seismic performance of steel plate reinforced concrete shear wall and its application in China Mainland. J Constr Steel Res 2017;131:132–43.
[7] CMC. Technical specification for concrete structures of tall building (JGJ 3-2010). Beijing: China Ministry of Construction; 2011. [in Chinese].
[8] Hu HS, Nie JG, Fan JS, et al. Seismic behavior of CFST-enhanced steel plate-reinforced concrete shear walls. J Constr Steel Res 2016;119:176–89.
[9] Guo LH, Rong Q, Qu B, Liu JP. Testing of steel plate shear walls with composite columns and infill plates connected to beams only. Eng Struct 2017;136:165–79.
[10] Zhao QH, Astaneh-Asl A. Cyclic behavior of traditional and innovative composite shear walls. J Struct Eng 2004;130(2):271–84.
[11] Rassouli B, Shafaei S, Ayazi A, Farahbod F. Experimental and numerical study on steel-concrete composite shear wall using light-weight concrete. J Constr Steel Res 2016;126:117–28.
[12] Dong HY, Cao WL, Wu HP, Qiao QY, Yu CP. Experimental and analytical study on seismic behavior of steel-concrete multi energy dissipation composite shear walls. Earthq Eng Eng Vib 2015;14(125–13):9.
[13] CMC. Technical specification for concrete structures of tall building (JGJ 3-2011). Beijing: China Ministry of Construction; 2011. [in Chinese].
[14] CMC. Code for design of concrete structures (GB 50010-2010). Beijing: China Ministry of Construction; 2010. [in Chinese].
[15] AIJ. Recommendations for design and construction of concrete filled steel tubular structures. Architecture Institution of Japan; 2008. [in Japanese].
[16] CMC. Code for design of steel structures (GB 50017-2003). Beijing: China Ministry of Construction; 2010. [in Chinese].
[17] DD ENV. Eurocode 4: Design of composite steel and concrete structures, Part 1.1: General rules and rules for buildings (together with United Kingdom National Application Document). London W1A2BS: British Standards Institution; 1994.
[18] CMC. Code for design of composite structure (JGJ 138-2012). Beijing: China Ministry of Construction; 2012. [in Chinese].
[19] CMC. Specification of testing methods for earthquake resistant building (JGJ. 101-96). Beijing: China Ministry of Construction; 1997. [In Chinese].
[20] Park R. Evaluation of ductility of structures and structural assemblages from laboratory testing. Bulletin of the New Zealand National Society for Earthquake Engineering; 1989.
[21] Zhang HM, Lu XL, Lu L, Cao WQ. Influence of boundary element on seismic behavior of reinforced concrete shear walls. J Earthq Eng Eng Vib 2007;27(1):92–8.
[22] Todut C, Dan D, Stoian V. Theoretical and experimental study on precast reinforced concrete wall panels subjected to shear force. Eng Struct 2014;80:323–38.